Dynamics of grain ejection by sphere impact on a granular bed

S. Deboeuf,[1,2] P. Gondret,[1] and M. Rabaud[1]

[1]*Univ. Paris-Sud, Univ. Paris 6, CNRS, Lab. FAST, UMR 7608, Bâtiment 502, Campus Universitaire, 91405 Orsay, France*

[2]*Univ. Paris 6, Univ. Paris 7, CNRS, Lab. de Physique Statistique de l'Ecole Normale Supérieure,*
UMR 8550, 24 rue Lhomond, 75231 Paris Cedex 05, France

The dynamics of grain ejection consecutive to a sphere impacting a granular material is investigated experimentally and the variations of the characteristics of grain ejection with the control parameters are quantitatively studied. The time evolution of the corona formed by the ejected grains is reported, mainly in terms of its diameter and height, and favorably compared with a simple ballistic model. A key characteristic of the granular corona is that the angle formed by its edge with the horizontal granular surface remains constant during the ejection process, which again can be reproduced by the ballistic model. The number and the kinetic energy of the ejected grains are evaluated and allow for the calculation of an effective restitution coefficient characterizing the complex collision process between the impacting sphere and the fine granular target. The effective restitution coefficient is found to be constant when varying the control parameters.

PACS number(s): 45.70.−n, 45.50.−j, 83.80.Fg, 96.15.Qr

I. INTRODUCTION

Impact cratering has been recognized as an important geological process for the last decades when the lunar craters have been finally attributed to impact structures rather than giant volcanoes as believed until 1950s [1]. The planetary impact craters such as the ones observed commonly on the Moon or the Earth result from very high energy impacts of meteorites and thus involve numerous and very complex phenomena such as shock and rarefaction wave propagation, melt, and vaporization of the projectile and target materials, together with excavation by displacement and ejection of the target material [1]. With so high energy, the material strength of any planet surface is negligible, so that laboratory scale experiments were conducted on noncohesive granular materials [2,3]. Since a few years, physicists have also conducted laboratory scale experiments on granular matter but with rather low impact energy, interested in the crater morphology, and searching for scaling laws for the crater size [4–7]. In these impact experiments, physicists have also been interested in the penetration of the impacting sphere in the granular target [8–14]. Indeed, despite recent progress on the complex rheology of granular matter [15], the penetration dynamics of a solid sphere into a granular medium is still difficult to understand well as it involves both the complex drag resulting from frictional and collisional processes, and the final stop involving the complex "liquid-solid" transition exhibited by granular matter [16]. The penetration dynamics of the impacting sphere and the grain ejection have been shown to be very different when the granular material is not dense but loose: a spectacular thin granular jet can rise very high after the impact as first demonstrated in Refs. [2,17,18]. The effects on this granular jet of the interstitial fluid [19,20] and of the initial packing fraction of the target [21] have then been studied. In the dense case, no granular jet but a growing granular corona is seen after the impact. These different kinds of grain ejection can be related to similar kinds of liquid ejection consecutive to the impact of a droplet into a deep or thin layer of liquid that have been first filmed by [22]

and then studied extensively [23,24]. Much less studies focusing on the grain ejection have been performed in the dense granular case: Ogale *et al.* [25] measured the mass of the spilled-over grains and Boudet *et al.* [26] proposed a model of ejection for the crater growth in a layer of thickness small compared to the size of both projectile and target grains at low impact velocities (∼1 m/s), while Cintala *et al.* [27] measured ejection speeds and angles of grains at high impact velocities (∼1 km/s). Another type of experiments concern the impact of one bead with a granular target made of the same beads [28]. Such impacts and grain ejections by an impacting projectile have been recently simulated in limiting cases, for which the impact energy is very low or very high [29,30] or for which the projectile size is about the grain size [31–33]. We focus in the present paper on the dynamics of the granular corona formed by the ejected grains from a dense and deep pile upon low speed (∼1 m/s) impacts. In Sec. II, the experimental setup is described together with the measurements. A simple ballistic model where grains are ejected locally in space with rapid time decreasing velocities is then presented in Sec. III and compared to the experimental data and also to the Maxwell *Z* model used for cratering flow [1,34]. The different scaling laws obtained for the ejection process are then discussed and compared in Sec. IV with known scaling laws for crater sizes.

II. EXPERIMENTS

Each experimental run consists of dropping a solid sphere into a granular medium. Four different steel spheres of density $\rho_s = 7800$ kg/m^3 are used as impactors with different radii $R = 5.15$, 6.75, 7.55, and 9.50 mm and masses M ranging thus from 4.5 to 30 g. The steel sphere is initially held by a magnet through a semispherical hole, so that the sphere can be dropped without any translational or rotational velocity by pulling up the magnet. The sphere is released directly above the center of a container and falls along its axis. Being dropped from the height h above the granular surface which

is varied between 8 and 60 cm, the sphere thus impacts the granular material with the velocity U_c varying from 1 to 4 m/s and energy $E_c = Mgh$ ranging from 3×10^{-3} to 2×10^{-1} J. The target material consists in sieved glass beads of density $\rho_g = 2500$ kg/m^3 ($\rho_s/\rho_g = 3.1$) and mean diameter $2r = 0.4 \pm 0.1$ mm ($R/r \sim 25-50$), thus of mass $m = 8 \times 10^{-5}$ g ($M/m \sim 10^4 - 10^5$). The granular material fills a cylindrical container of diameter of 19 cm and height of 26 cm. The size ratio of the container diameter over the sphere diameter is always larger than 10, so that there is no influence of the radial confinement by the lateral walls neither of the bottom walls of the container as the height of the packing is large [13]. Before each drop, the granular medium is prepared by gently stirring the grains with a thin rod. The container is then overfilled and the surface leveled using a straight edge. The typical value of the solid volume fraction of the packing is $(62 \pm 1)\%$. Each impact experiment is lighted from the front to enhance contrast between the grains and the black background, and side-view images are recorded by a high-speed camera at the rate of 500 images per s ($\Delta t = 2$ ms) and resolution of 0.16 mm per pixel.

Figure 1 shows a sequence of side-view images separated by 30 ms illustrating the ejection dynamics of the grains after the time $t = 0$ defined as the first contact between the bottom of the sphere and the granular surface. One can see few isolated ejected grains above a dense corona of grains that expands vertically and radially. The amount of ejected grains, which is one of the pertinent physical quantities that can be estimated by measuring, after thresholding the video images, the apparent surface area A_{tot} of all the grains in each image. The evolution of A_{tot} as a function of time is reported in Fig. 2 for several experiments corresponding to different dropping heights h of the same sphere. After impact A_{tot} increases up to a maximal value denoted $A_{\mathrm{tot\ max}}$ at the time $t_{A_{\mathrm{tot\ max}}}$ before decreasing. Each curve corresponds to a single-impact experiment, thus without any ensemble averaging, but with a little smoothing by a slide average over a time window of 10 ms, so that no data appear before $t = 4$ ms in the reported figures. Increasing the dropping height h of a given sphere, the values $A_{\mathrm{tot\ max}}$ and $t_{A_{\mathrm{tot\ max}}}$ increase, accounting for the increase in both the number of ejected grains and the dynamics duration. The same goes when keeping constant the dropping height h and increasing the mass M of the impacting sphere. It is worth noting that the exact relation between the measured apparent surface area A_{tot} of the ejected grains and the real total number of ejected grains N_{ej} is not straightforward. For dilute zones of ejected grains, all the grains can be seen in the two-dimensional (2D) images, but there is still the problem of focusing: a far grain appears smaller than a close grain, so that the grains do not have the same apparent area. The most problematic case concerns however the dense zones where some grains can be hidden by other grains. Using the fact that the ejection process is axisymmetric, the number of ejected grains N_{ej} may be however related to the measured apparent surface area $A_{\mathrm{tot\ max}}$ by

$$N_{ej} = \bar{n}\bar{w}\pi A_{\mathrm{tot\ max}}, \qquad (1)$$

where $\bar{n}$ is the unknown mean number of grains per unit volume in the corona and $\bar{w}$ is the mean unknown corona
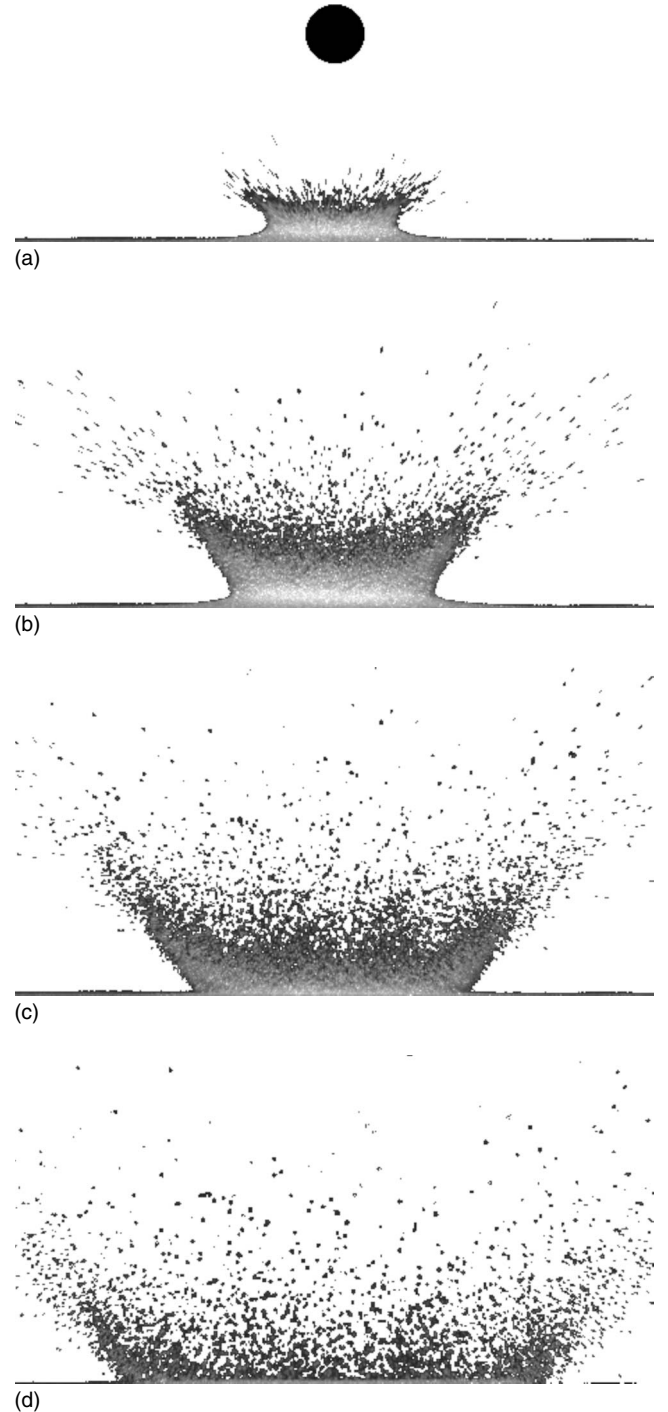

(a)

(b)

(c)

(d)

FIG. 1. Sequence of side-view images separated by 30 ms (with first image corresponding to $t = 10$ ms), showing the typical time evolution of ejected grains after the impact of a steel sphere of radius $R = 6.75$ mm dropped from the height $h = 30$ cm ($U_c = 2.45$ m/s, $E_c = 30$ mJ). To give the scale, a black disk of the same radius as the sphere is shown in the first frame.

thickness. The unknown product $\bar{n}\bar{w}$ will be deduced in Sec. IV by comparing our scaling laws for the grain ejection with scaling laws already known in the literature for the crater size.

In impact experiments of a drop onto a liquid layer, a beautiful corona is classically observed [22,24]. In such a
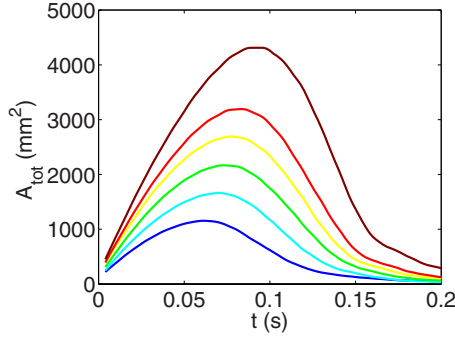
FIG. 2. (Color online) Time evolution of the total apparent surface of ejected grains A_{tot} for an impacting steel sphere of radius $R = 7.55$ mm dropped from different heights $h = 13, 23, 33, 43, 48$, and 58 cm (from bottom to top).

liquid case, the corona is easy to define and extract as the liquid is a continuous medium. In the granular case, the corona is less easy to define as the ejected grains are individual entities. The granular corona is here defined as the largest visually connected grains in each side-view image obtained after thresholding and binarization of the raw video image. We have checked that the size of the corona does not depend significantly on the lighting and contrast of the images. To investigate the time evolution of the corona and characterize its shape, which is basically axisymmetric, its contour is extracted by applying an edge detection algorithm to each image. An example of such a contour is drawn in Fig. 3. Note that this corresponds to the external contour of the ejecta curtain. This allows us to measure the bottom diameter D_b and the top diameter D_t as the minimal and maximal diameters of the corona. The height H of the corona is measured as the distance between the mean vertical position of the corona top contour (light gray line on Fig. 3, red online) and the granular surface level before impact. As the corona lateral edge appears quite straight except in a small zone at the base of the corona, we determine also the angle θ formed by the corona edge (light gray line on Fig. 3, green online) with the horizontal by a linear fit through the straight portion.

The time evolution of the corona, in terms of its height H, its top and bottom diameters D_t and D_b, and its edge slope θ, is displayed in Fig. 4 for the same experiments as in Fig. 2. The expansion of the corona is demonstrated in Fig. 4(a) by the increase in its height H up to a maximal value denoted H_{max} at time $t_{H_{max}}$ before decreasing. For a given sphere,
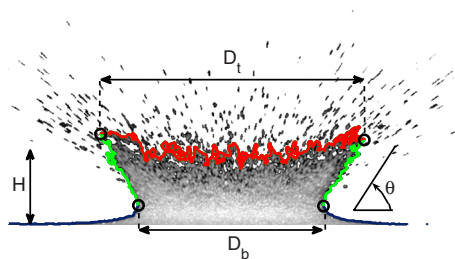

FIG. 3. (Color online) Geometrical parameters characterizing the corona of ejected grains: the bottom and the top diameters D_b and D_t of the corona, its height H, and its edge angle θ. They are automatically extracted from the contour of the corona (see text).
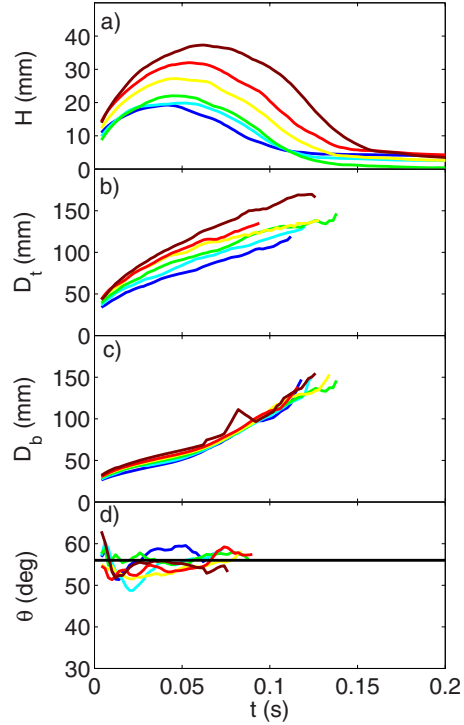

FIG. 4. (Color online) Time evolution of (a) the height H, (b) the top diameter D_t, (c) the bottom diameter D_b, and (d) the angle of the corona θ for the same experimental parameters as in Fig. 2. The horizontal line in (d) is the time and ensemble average of $\theta(t)$ for the 65 experiments.

H_{max} and time $t_{H_{max}}$ increase monotonically with the dropping height h, so that the different curves of Fig. 4(a) appear in order. Note that for large impact energies (large impact heights h), H decreases to a significant nonzero final value because of the final crater rims lying above the initial free surface [4]. As time is extrapolated back to zero, it can be noticed that H does not vanish smoothly. We believe that this is related to a rapid initial swelling of the granular bed that may be observed at the very first instants of penetration, not resolved here with our video camera as between two successive images separated by $\Delta t = 2$ ms, the sphere falls typically one radius. In the same time, the top diameter D_t and the bottom diameter D_b increase with time up to a maximal value, as shown in Figs. 4(b) and 4(c), but the curvatures of $D_t(t)$ and $D_b(t)$ seem somewhat different. Besides, D_t increases significantly with the dropping height h whereas D_b does not vary so much. Note that at the nearly end of the corona life, for vanishing height H, the values of D_t and D_b become very noisy and are thus not shown here. As time is extrapolated back to zero, it can be noticed that D_t and D_b decrease roughly toward the projectile diameter meaning that the ejection process takes place close to the projectile. The angle θ the corona edge forms with the horizontal, shown in Fig. 4(d), is roughly constant in time and whatever the dropping height h, and equal to about 56° with relative variations of $\sim 5\%$. The same kind of evolutions of all these parameters is observed for the different tested spheres.

The corona evolution reported here for granular impacts can be compared to the corona evolution for the liquid case.
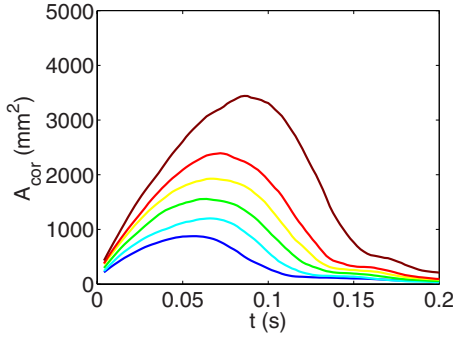
FIG. 5. (Color online) Time evolution of the apparent surface area of the corona A_{cor} for the same experimental parameters as in Fig. 2.

For the liquid case, the corona base D_b spreads radially as the square root of time [24]. For the granular case, even if an initial $t^{1/2}$ growth may exist for geometrical reasons at the very first instants not resolved here, the following evolution seems more quadratic [see $D_b(t)$ in Fig. 4(c)]. Besides, the angle of the granular corona is found independent of the impact velocities, as found for the liquid corona, with a value closer to the case of shallow liquid layers than the case of deep liquid layers [23]. This may be related to the collisional chains existing in granular layer that redirected the impact velocity within a few grains layer only [32].

With the measurements of the geometrical parameters of the corona, we can now define the apparent area of the corona A_{cor} that is related to the amount of ejected grains contained in the corona and compare it to the total apparent area of ejected grains A_{tot}, related to the total amount of the ejected grains, both in the corona and isolated. A_{cor} is measured as the area included inside the corona contour, which is not far from the area $H(D_t+D_b)/2$ corresponding to the approximate corona trapezium shape in the images. The time evolution of A_{cor} is reported in Fig. 5 for the same experimental parameters as in Figs. 2 and 4. Even if A_{cor} is always smaller than A_{tot}, the evolution of A_{cor} is qualitatively the same as the one of A_{tot} (Fig. 2). This is confirmed by the quantitative comparison of the corresponding coordinates of the curve maxima, $(t_{A_{tot\ max}}, A_{tot\ max})$ and $(t_{A_{cor\ max}}, A_{cor\ max})$,

that are reported in Fig. 6 for all the experiments (all dropping heights and all different impacting spheres). The evolutions of A_{cor} and A_{tot} are synchronized in time as illustrated by the equality $t_{A_{cor\ max}} \simeq t_{A_{tot\ max}}$ [Fig. 6(a)]. Besides, $A_{cor\ max}$ is found proportional to $A_{tot\ max}$ with the same ratio for all experiments: $A_{cor\ max} \simeq 0.75 A_{tot\ max}$ [Fig. 6(b)]. Let us now interpret these experimental results on the corona dynamics by a simple ballistic model.

III. BALLISTIC MODEL FOR GRAIN EJECTION

In the 1970s, Maxwell [34] introduced a simple phenomenological model for the cratering flow induced by a near surface explosion. In this model, now called the Maxwell Z model [1], the radial velocity field in the ground decreases with the distance to impact r as r^{-Z} and it is completed by a tangential velocity field that insures the incompressibility of the flow. For an explosion close to the surface, this model predicts that materials will be ejected from the surface at the same time, with the same angle $\alpha = \tan^{-1}(Z-2)$, and a velocity modulus decreasing as $u_0(r/r_0)^{-Z}$ for $r \geq r_0$. A ballistic model following this initial condition predicts the transient formation of a corona. Such a model gives interesting results for the description of planet craters using the adjustable parameters r_0, u_0, and Z with $2<Z<4$ even if a large number of improvements of this model have been tested since. In the following we interpret our results with an even simpler ballistic model where all the grains are ejected at a given radius, with different velocities.

In the present results the dynamics of the grains is found axisymmetric and rapidly contact forces between grains play no role (Fig. 1). Furthermore air friction can be estimated and is completely negligible compared to the grain weight. Thus rapidly after impact, each grain trajectory corresponds to a parabolic free flight under the action of gravity alone. Using these preliminary remarks, we now build a very simple axisymmetric model that reproduces the observed corona dynamics in the (r,z) plane of cylindrical coordinates.

As a first attempt, we assume that all grains start at the same time $t=0$, from the same position $(r_0,0)$, in the same initial direction making an angle α with the horizontal, but with different velocity amplitudes. It is thus easy to show

(a)

(b)
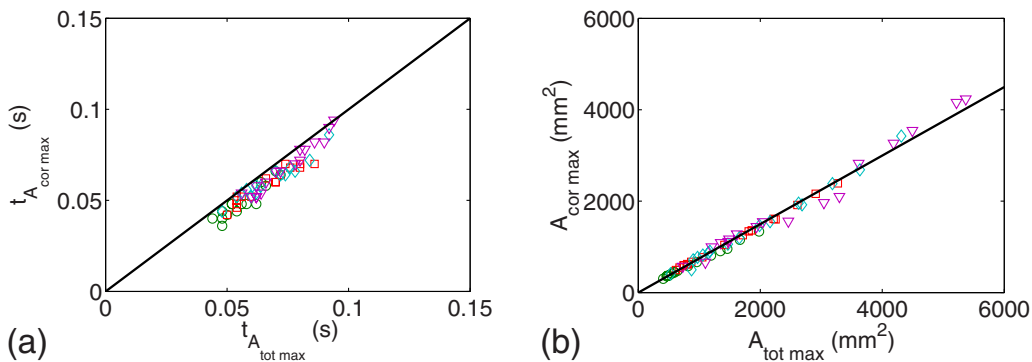
FIG. 6. (Color online) (a) Time $t_{A_{cor\ max}}$ for maximal value of the corona apparent area A_{cor} as a function of time $t_{A_{tot\ max}}$ for maximal value of the total apparent area A_{tot}. The solid line is of slope 1. (b) Maximal values $A_{cor\ max}$ of A_{cor} as a function of maximal values $A_{tot\ max}$ of A_{tot}. The solid line is a linear fit. Data symbols are for the 65 experiments with different dropping heights h for impacting spheres of radius $R=5.15$ (○), 6.75 (□), 7.55 (◇), and 9.50 (▽).
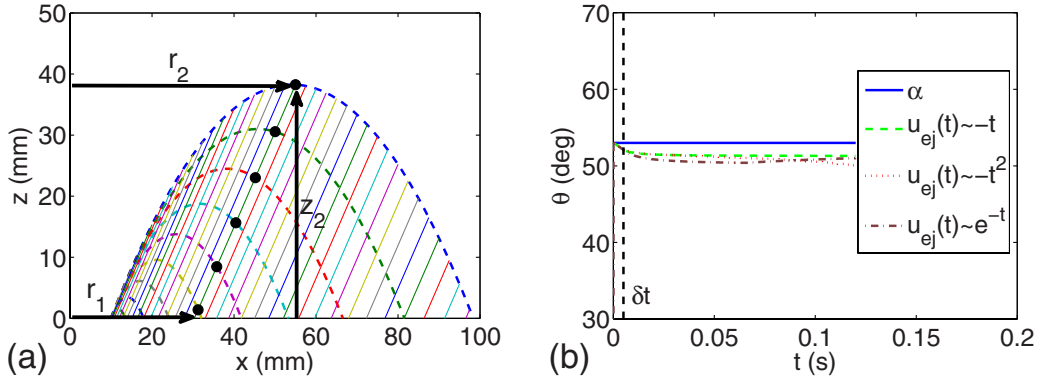
FIG. 7. (Color online) (a) Ballistic model for grains ejected instantaneously from the same position $r_0 = 10$ mm in the same direction making the angle $\alpha = 53°$ with the horizontal, with different velocity amplitudes. Trajectories are drawn in dashed lines. At any time grains align along a straight line forming the corona edge of angle $\theta = \alpha$ drawn in continuous lines. (b) Time evolution of the angle θ of the cone edge if grains are ejected during a finite time $\delta t = 5$ ms in the direction $\alpha = 53°$, with a linear, quadratic, or exponential decrease in ejection velocity from the initial value $u_0 = 1$ m/s.

[Fig. 7(a)] that at any following time t all the grains will be located on a cone making the same angle α with a bottom diameter $2r_1$ increasing quadratically with time as $2r_1(t) = 2r_0 + gt^2/\tan \alpha$. Furthermore, if u_0 is the maximal amplitude of initial velocity, the top diameter of the cone $2r_2$ increases linearly with time as $2r_2(t) = 2r_0 + 2u_0 \cos \alpha t$ and the height of the cone z_2 evolves quadratically in time as $z_2(t) = u_0 \sin \alpha t - gt^2/2$. These analytical results are quite similar to the dynamics observed in Fig. 1 and to the time evolution of the corona parameters H, D_t, D_b, and θ presented in Fig. 4. The hypothesis of an instantaneous release of all the grains at the same place and the same time $t = 0$ is however clearly oversimplified. Indeed grains are ejected during a time interval δt on the order of the penetration time $R/U_c \sim 5$ ms, and as the projectile decelerates the ejection velocity of the grains should be a decreasing function of time. In Fig. 7(b), we plot the apparent cone angle $\theta(t)$ of the moving grains when released with the same ejection angle α but with various models of time decreasing velocities $u_{ej}(t)$ during the time interval $\delta t = 5$ ms: a linear decrease $[u_{ej}(t) = u_0(1 - t/\delta t)]$, a quadratic decrease $[u_{ej}(t) = u_0(1 - t^2/\delta t^2)]$, or an exponential decrease $[u_{ej}(t) = u_0 \exp(-t/\delta t)]$ from the initial value $u_0 = 1$ m/s. Except at very short times the edge angle θ remains constant and always close to the ejection angle α. While the time evolutions for the top diameter $2r_2$ and the height z_2 of the apparent cone are obviously the same as for an instantaneous release, it appears to be also the same but with a small delay time δt for the bottom diameter $2r_1$. As this delayed grain ejection and initial velocity decrease have no significant effect in the corona dynamics, we will use in the following the first simpler model where all the grains are ejected *at the same time* with ejection velocities in the range $0 \leq u_{ej} \leq u_0$.

In the experiments we measured the time evolution of the corona parameters, i.e., the optically opaque zone formed by ejected grains, when viewed from the side. The relation between this corona that corresponds to a 2D projection of the three-dimensional (3D) real dynamics and the latter is not straightforward. But the bottom diameter D_b and the edge angle θ are clearly the same. Furthermore, Fig. 6 shows that most of the grains are inside the corona. In the following we

will then consider that the height H and the top diameter D_t of the corona in the experiments are identical to the height z_2 and the top diameter $2r_2$ of the cone in the ballistic model. Assuming this, the time evolution of H, D_t, D_b, and θ are given by the following set of equations:

$$H(t) = u_0 \sin \alpha t - gt^2/2 + H(0), \tag{2a}$$

$$D_t(t) = D_t(0) + 2u_0 \cos \alpha t, \tag{2b}$$

$$D_b(t) = D_b(0) + gt^2/\tan \alpha, \tag{2c}$$

$$\theta = \alpha. \tag{2d}$$

An initial height $H(0)$ has been introduced in the dynamics of $H(t)$ as we observe in the experiment an initial swelling of the granular bed before any grain ejection. This swelling corresponds to a deformation of the substrate when the projectile starts to penetrate the bed. This deformation process is clearly not contained in our ballistic description and it is not well time resolved with our video camera. The horizontal position of ejection r_0 is related to the projectile size: we checked that $D_t(0)$ and $D_b(0)$ increase with the impacting sphere diameter $2R$. The set of equations (2a)–(2c) can be written in dimensionless form as

$$\frac{H(t) - H(0)}{H_{max} - H(0)} = 2\left(\frac{t}{t_{H_{max}}}\right) - \left(\frac{t}{t_{H_{max}}}\right)^2, \tag{3a}$$

$$\frac{D_t(t)}{D_t(0)} = 1 + \frac{2u_0 \cos \alpha}{D_t(0)}t, \tag{3b}$$

$$\frac{D_b(t)}{D_b(0)} = 1 + \frac{g}{D_b(0)\tan \alpha}t^2 \tag{3c}$$

with the two scaling parameters $t_{H_{max}} = u_0 \sin \alpha/g$ and $H_{max} - H(0) = gt_{H_{max}}^2/2$.

For each of the 65 experiments, our experimental data for the height $H(t)$ and the top diameter $D_t(t)$ of the corona are rather well fitted by the ballistic model equations as shown in
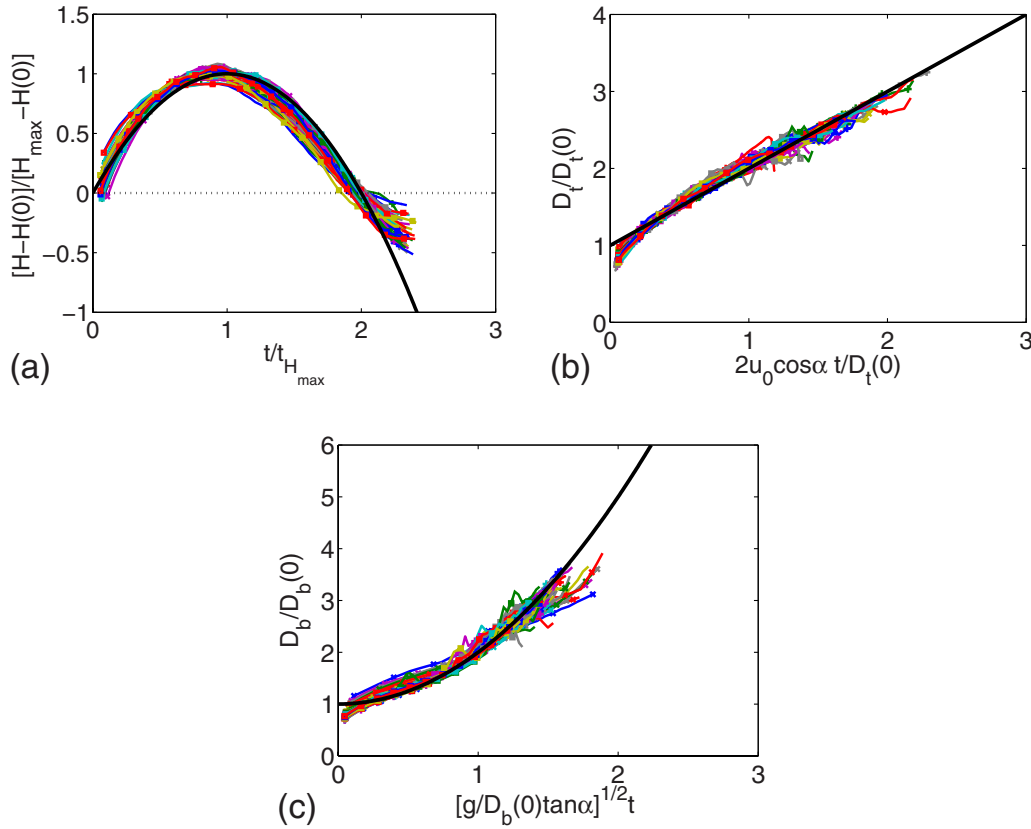
FIG. 8. (Color online) Rescaled data of (a) heights $[H-H(0)]/[H_{\max}-H(0)]$, (b) top diameter $D_t/D_t(0)$, and (c) bottom diameter $D_b/D_b(0)$ as a function of rescaled times appearing in Eq. (3) for all of the 65 experiments.

the nondimensional plots of Figs. 8(a) and 8(b). The evolution of H is basically quadratic, while D_t is rather linear in time. The fitting parameters $u_0 \sin \alpha$ for $H(t)$ and $u_0 \cos \alpha$ for D_t give access to the typical grain ejection velocity u_0 and to the typical ejection angle α for each impact experiment. The time evolution of the bottom diameter of the corona $D_b(t)$ is shown in the nondimensional plot of Fig. 8(c), with the already deduced fitting parameters: the predicted quadratic increase in D_b is rather well followed by the experimental data. The fitted angle of ejection α is found constant for all experiments: $\alpha \simeq 53° \pm 3°$, which corresponds well to the corona edge angle $\theta \simeq 56° \pm 3°$ measured previously [Fig. 4(d)]. We have checked that α and θ are robustly constant for all experiments and do not depend on any impact parameter, as shown in Fig. 9: no clear correlation of α with the impact energy E_c can be seen. The equality found between the fitted ejection angle α and the measured corona edge angle θ is again in favor of the present grain ejection scenario.

Note that if we analyze our results in terms of the Maxwell Z model, the measured angle of the corona imposes the value $Z=3.4$. This relatively large value of Z imposes that the ejected grains are located very close to r_0. Because of the radial extension of the initial velocity field, this model is able to describe the finite curvature observed initially at the base of the corona (see Fig. 3) and that our simpler model does not catch. Anyway both models give good results because experimentally the ejected grains are well localized both in

space $[\Delta r_0 \ll D_b(t_{\max})]$ and time $(\delta t \ll t_{\max})$, with a continuous range of initial velocity $[0, u_0]$.

From Eqs. (2a)–(2c), we can calculate the area of the corona $A_{\text{cor}}(t)$: the predicted evolution is in good agreement with experimental results and gives $t_{A_{\text{cor max}}} = 1.36 t_{H_{\max}}$ very close to the coefficient of 1.38 measured experimentally.

Although we do not measure directly the grain ejection velocities, the fits of Fig. 8 give a characteristic ejection velocity u_0. Figure 10(a) shows the slow increase in u_0 with the impact velocity U_c and its dependence on the sphere radius, where we can see that U_c is not the relevant parameter to account for the variations of u_0. The data collapse on
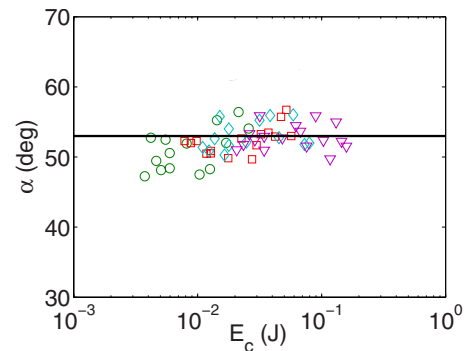

FIG. 9. (Color online) Fitted ejection angle α as a function of the impact energy E_c for the 65 experiments (same symbols as in Fig. 6).
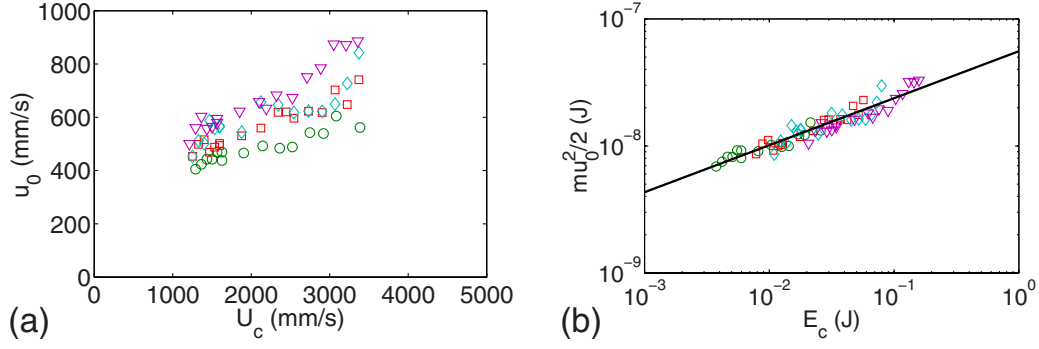
FIG. 10. (Color online) Variations of ejection parameters with the impact parameters: (a) Ejection velocity u_0 as a function of impact velocity U_c and (b) kinetic energy of one grain $mu_0^2/2$ as a function of impact energy E_c and the best power-law fit (4). Same symbols as in Fig. 6.

Fig. 10(b), where the kinetic energy of one ejected grain $mu_0^2/2$ is plotted as a function of the kinetic impact energy $E_c=MU_c^2/2$ in log-log axes, shows that E_c is the relevant parameter. The collapse corresponds to the power law

$$mu_0^2/2 \simeq 0.56 \times 10^{-9} E_c^{0.37 \pm 0.05}, \qquad (4)$$

showing a moderate effect of the impact energy on the kinetic energy of one ejected grain. From the ballistic model presented above and this experimental result of the scaling of the ejection velocity u_0 with the impact energy E_c, we can infer the scalings for the total duration of the corona ballistic dynamics T, for its maximal height $H_{\max}$ and its maximal top diameter $D_{t \max}$ with the impact energy E_c as

$$T = 2t_{H_{\max}} = 2u_0 \sin \alpha/g \propto E_c^{0.19}, \qquad (5)$$

$$H_{\max} = g t_{H_{\max}}^2/2 = u_0^2 \sin^2\alpha/2g \propto E_c^{0.37}, \qquad (6)$$

$$D_{t \max} = u_0^2 \sin 2\alpha/g \propto E_c^{0.37}, \qquad (7)$$

allowing us to characterize the duration and the extension of deposits upon an impact. These results show that the corona duration T depends only slightly on the impact energy E_c, whereas the corona expansion depends moderately on E_c.

In Eq. (1), the characteristic number of ejected grains N_{ej} has been related to the maximal value of the total apparent

surface of all the ejected grains $A_{\text{tot max}}$ through the unknown product $\bar{n}\bar{w}$. We will see in Sec. IV that $\bar{n}\bar{w} \simeq 12$ mm^{-2} and we thus use from now on this value to calculate the number of ejected grains N_{ej} according to Eq. (1). In Fig. 11(a) N_{ej} is plotted as a function of the impact energy E_c in log-log axes. We see that, whatever the projectile size, all the data collapse close to the power law

$$N_{ej} \simeq 7.2 \times 10^5 E_c^{0.70 \pm 0.05}. \qquad (8)$$

We can now estimate an upper bound for the kinetic energy transmitted to all the ejected grains as $E_{ej} \simeq N_{ej} m u_0^2/2$. Figure 11(b) shows the evolution of E_{ej} as a function of E_c. The total kinetic energy of the ejected grains is found proportional to the impact energy as

$$E_{ej} \simeq 0.031 E_c. \qquad (9)$$

This unexpected result allows for the definition of a constant effective restitution coefficient $\epsilon = \sqrt{E_{ej}/E_c} \approx 0.18$. The small value of ϵ confirms the well-known and well-used fact that granular beds are very efficient dissipating systems.

IV. DISCUSSION

In this paper, we have shown that the number of ejected grains N_{ej} obeys a scaling law with the impact energy E_c [see
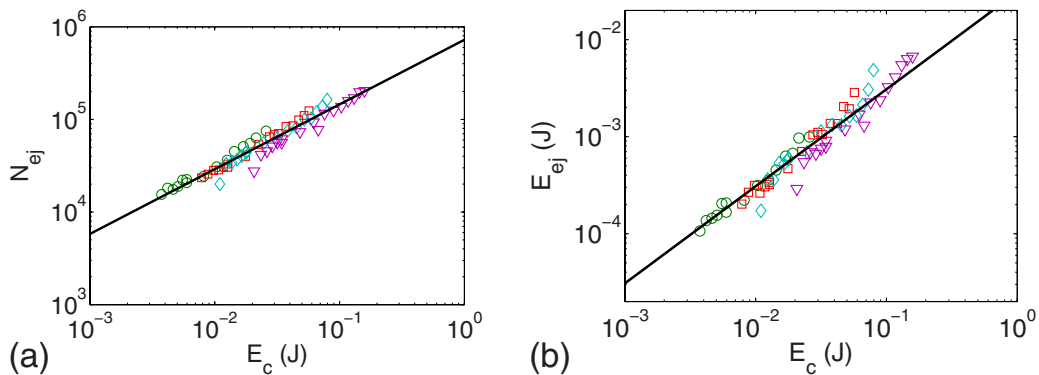

FIG. 11. (Color online) (a) Number of ejected grains N_{ej} as a function of impact energy E_c for all experiments, and best power-law fit given in Eq. (8). (b) Kinetic energy of ejecta E_{ej} as a function of impact energy E_c and best power-law fit given in Eq. (9). Same symbols as in Fig. 6.

Eq. (8)]. In the literature, the impact energy has been shown to be also the relevant parameter that governs the crater size, in terms of its typical radius and depth [4–7]. Let us now relate these different scaling laws. The scaling laws known from Ref. [7] for the typical radius R_{crat} and depth H_{crat} of craters are $R_{crat} \propto E_c^{0.23}$ and $H_{crat} \propto E_c^{0.21}$. The volume V of craters can thus be also related to the impact energy as $V \sim H_{crat}R_{crat}^2 \propto E_c^{0.67}$, with a numerical prefactor that depends on the precise shape of the crater and on the grain and projectile properties. From the crater profile measurements of Ref. [7] for glass beads, we deduce the precise scaling law for the crater volume as follows:

$$V \simeq 3.6 \times 10^4 E_c^{0.67}. \qquad (10)$$

From this expression for the crater volume, we can estimate the number of grains that have been ejected as $N_{crat} = V\Phi/v$, where $v = 4\pi r^3/3$ is the volume of one grain and Φ is the solid volume fraction of the granular packing ($\Phi \simeq 0.6$). This number of excavated grains follows thus a power law with the impact energy with the exponent 0.67 that is very close to the exponent 0.70 measured here for the ejected grains in Eq. (8). This definitely confirms that the geometrical measurements made on the corona give relevant and quantitative information on the grain ejection dynamics. Writing that the number of ejected grains N_{ej} measured here is equal to the number of excavated grains N_{crat} from [7] allows us to bypass the unknown prefactor $\bar{n}\bar{w}$ in Eq. (1) and to accurately calculate N_{ej} and E_{ej} shown in Fig. 11: imposing the equality $N_{ej} = N_{crat}$ gives $\bar{n}\bar{w} \simeq 12$ mm^{-2}.

The scaling laws $u_0 \propto E_c^{0.18}$ and $N_{ej} \propto E_c^{0.70}$ obtained here for a large projectile over grain size ratio ($R/r \sim 25$–50) are close to the results obtained for a small size ratio ($R/r = 1$) in [28]: $\bar{u}_0 \propto E_c^{0.12}$ and $\bar{N}_{ej} \propto E_c^{0.75}$, where $\bar{u}_0$ and $\bar{N}_{ej}$ refer to ejection velocity and number of ejected grains averaged over many experiments. This suggests that the same scaling laws hold whatever the ratio R/r is. The constant value of the ejection angle equal to about $55° \pm 5°$ is in agreement with previous values measured between $40°$ and $60°$ in the case of high-speed impacts [27,30].

Let us recall that the energy of the ejected grains is shown to correspond to a maximum of 3% of the impact energy [Eq. (9)], which is much larger than the tiny fraction (0.3% ac-

cording to [7]) required to excavate the crater, i.e., for the grains to move just above the granular surface with zero velocity. This is illustrated by the larger values of the maximal height of the corona H_{max} [between 10 and 40 mm in Fig. 4(a)] than the values of crater depth (between 4 and 10 mm in [4,7]) for the same material properties and impact conditions. This suggests us to take into account the kinetic energy of the ejected grains when considering balance of energies. However the essential part ($\sim$97%) of the impact energy is dissipated in the granular target through frictional contacts and inelastic collisions.

V. CONCLUSION

The dynamics of grain ejection due to a large sphere impacting a granular material has been experimentally investigated through the time evolution of the corona, mainly in terms of its geometry. Whereas the dimensions of the corona—its height and top and bottom diameters—change with time, the angle formed by its edge with the horizontal granular surface remains constant during the ejection process. All these geometrical properties are well described by a simple ballistic model, supporting that grains are quasi-instantaneously ejected at impact from a rather localized radial position. This direction appears to be constant when varying the experimental parameters and equal to about $55°$. By contrast, the typical ejection velocities and number of ejected grains change when varying experimental parameters and are controlled by the impact energy through power laws. The estimate of the energy of ejected grains allows finally for the calculation of an effective coefficient of restitution characterizing the complex collision process between the impacting sphere and the fine granular target. An important result is that this effective restitution coefficient is constant when varying the experimental parameters and very small. For the present packing fraction, 97% of the impact energy is dissipated during the collision process.

[1] H. J. Melosh, *Impact Cratering: A Geologic Process* (Oxford University Press, New York, 1989).

[2] M. A. Cook and K. S. Mortensen, J. Appl. Phys. **38**, 5125 (1967).

[3] S. Yamamoto, K. Wada, N. Okabe, and T. Matsui, Icarus **183**, 215 (2006).

[4] A. M. Walsh, K. E. Holloway, P. Habdas, and J. R. de Bruyn, Phys. Rev. Lett. **91**, 104301 (2003).

[5] J. S. Uehara, M. A. Ambroso, R. P. Ojha, and D. J. Durian, Phys. Rev. Lett. **90**, 194301 (2003).

[6] X. J. Zheng, Z. T. Wang, and Z. G. Qiu, Eur. Phys. J. E **13**, 321 (2004).

[7] S. J. de Vet and J. R. de Bruyn, Phys. Rev. E **76**, 041306 (2007).

[8] J. R. de Bruyn and A. M. Walsh, Can. J. Phys. **82**, 439 (2004).

[9] M. P. Ciamarra, A. H. Lara, A. T. Lee, D. I. Goldman, I. Vishik, and H. L. Swinney, Phys. Rev. Lett. **92**, 194301 (2004).

[10] M. A. Ambroso, C. R. Santore, A. R. Abate, and D. J. Durian, Phys. Rev. E **71**, 051305 (2005).

[11] M. Hou, Z. Peng, R. Liu, K. Lu, and C. K. Chan, Phys. Rev. E **72**, 062301 (2005).

[12] H. Katsuragi and D. J. Durian, Nat. Phys. **3**, 420 (2007).

[13] A. Seguin, Y. Bertho, and P. Gondret, Phys. Rev. E **78**,

010301(R) (2008).

[14] D. I. Goldman and P. Umbanhowar, Phys. Rev. E **77**, 021308 (2008).

[15] G. D. R. Midi, Eur. Phys. J. E **14**, 341 (2004).

[16] P. Mills, P. Rognon, and F. Chevoir, EPL **81**, 64005 (2008).

[17] S. T. Thoroddsen and A. Q. Shen, Phys. Fluids **13**, 4 (2001).

[18] R. Mikkelsen, M. Versluis, E. Koene, G.-W. Bruggert, D. van der Meer, K. van der Weele, and D. Lohse, Phys. Fluids **14**, S14 (2002).

[19] J. R. Royer, E. I. Corwin, P. J. Eng, and H. M. Jaeger, Phys. Rev. Lett. **99**, 038003 (2007).

[20] G. Caballero, R. Bergmann, D. van der Meer, A. Prosperetti, and D. Lohse, Phys. Rev. Lett. **99**, 018001 (2007).

[21] J. O. Marston, J. P. K. Seville, Y.-V. Cheun, A. Ingram, S. P. Decent, and M. J. H. Simmon, Phys. Fluids **20**, 023301 (2008).

[22] A. M. Worthington, *A Study of Splashes* (Longmans, Green, and Co., London, 1908).

[23] A. I. Fedorchenko and A.-B. Wang, Phys. Fluids **16**, 3911 (2004).

[24] A. L. Yarin, Annu. Rev. Fluid Mech. **38**, 159 (2006).

[25] S. B. Ogale, S. R. Shinde, P. A. Karve, A. S. Ogale, A. Kulkarni, A. Athawale, A. Phadke, and R. Thakurdas, Physica A **363**, 187 (2006).

[26] J.-F. Boudet, Y. Amarouchene, and H. Kellay, Phys. Rev. Lett. **96**, 158001 (2006).

[27] M. J. Cintala, L. Berthoud, and F. Horz, Meteorit. Planet. Sci. **34**, 605 (1999).

[28] D. Beladjine, M. Ammi, L. Oger, and A. Valance, Phys. Rev. E **75**, 061305 (2007).

[29] L. S. Tsimring and D. Volfson, *Powders and Grains* (A. A. Balkema Publishers, Stuttgart, 2005), pp. 1215–1218.

[30] K. Wada, H. Senshu, and T. Matsui, Icarus **180**, 528 (2006).

[31] L. Oger, M. Ammi, A. Valance, and D. Beladjine, Eur. Phys. J. E **17**, 467 (2005).

[32] J. Crassous, D. Beladjine, and A. Valance, Phys. Rev. Lett. **99**, 248001 (2007).

[33] F. Bourrier, F. Nicot, and F. Darve, Granular Matter **10**, 415 (2008).

[34] D. E. Maxwell, in *Impact and Explosion Cratering*, edited by D. J. Roddy, R. O. Pepin, and R. B. Merrill (Pergamon Press, New York, 1977), pp. 1003–1008.